UDE-Based Trajectory Tracking Control of Piezoelectric Stages

Jinhao Chen, *Student Member, IEEE*, Beibei Ren, *Member, IEEE*, and Qing-Chang Zhong, *Senior Member, IEEE*

***Abstract*—The robust and precise control of piezoelectric stages is quite challenging due to the existence of strong hysteresis nonlinearity. In this paper, the dynamics of a piezoelectric stage is identified as a second-order linear system preceded by an input hysteresis characterized by the Prandtl–Ishlinskii (PI) model. Then, a control strategy based on the uncertainty and disturbance estimator (UDE) is developed to mitigate the effect of hysteresis nonlinearity and improve the performance of the positioning control of the piezoelectric stage, without the detailed model of the hysteresis except the slope information of the PI hysteresis asymptotes. Moreover, the stability analysis of the closed-loop system with the UDE-based controller is provided. Extensive experimental studies are carried out on a Physik Instrumente P-753.31c piezoelectric stage to demonstrate that the UDE-based controller can achieve excellent performance in trajectory tracking and disturbance rejection, compared to the proportional–integral–derivative (PID) controller and a disturbance-observer-based controller.**

***Index Terms*—Hysteresis, piezoelectric stage, Prandtl–Ishlinskii (PI), uncertainty and disturbance estimator (UDE).**

I. Introduction

PIEZOELECTRIC actuators are widely applied in both industrial and academic research, e.g., in nanopositioning, microrobotics, and active vibration control [1]–[5]. The popularity of piezoelectric actuators can be attributed to their inherent merits, including fast response, ultra-high resolution, high output force, large bandwidth, zero backlash, and little heat generation [6].

Despite the advantages of piezoelectric actuators, they generally exhibit strong hysteresis effects in their output response [7], which might cause inaccuracies, oscillations, and even instabilities in some closed-loop systems. Since the 1980s, it has been found that the hysteresis nonlinearities in charge-driven piezoelectric actuators are minimal [8], [9]. Therefore, the hysteresis effect can be eliminated or reduced by using a charge-driven approach or a capacitor-insertion method [10]. In [11] and [12], a new type of current and charge amplifier was proposed and analyzed. Nevertheless, this unique property of piezoelectric materials has not been widely used yet because it is difficult to drive highly capacitive loads with available charge/current amplifiers [13].

Compared to the charge control method, the voltage control method is more widely applied in practical piezo-actuated systems. Generally, most existing voltage control strategies are either model-based compensation or nonmodel-based compensation. For the first category, a suitable hysteresis model is needed for control design. Several phenomenological models have been proposed and widely used for modeling the hysteresis of piezoelectric actuators, e.g., Preisach model [14], [15], Prandtl–Ishlinskii (PI) model [7], [16]–[19], and Bouc-Wen model [20], [21]. Also, a polynomial-based hysteresis model was introduced in [22]. Typically, a corresponding inversion of the hysteresis model needs to be constructed for the feedforward control to compensate the hysteresis. The challenges with such approaches lie in the hysteresis modeling complexity and parameter sensitivity. It has been found that the hysteretic behaviors of piezoelectric materials might be varying with time, temperature, or some other ambient conditions [23]. In addition, some of the hysteresis models (e.g., Preisach model) are not analytically invertible, so only approximate inversions can be obtained. Thus, such inversion-based feedforward controllers are generally employed with other feedback controllers to achieve precise positioning control. In [15], a hysteresis compensator based on the inversion of Preisach model was combined with a proportional–integral–derivative (PID) controller to achieve robust control of a piezoelectric stage. For the second category, a feedback controller is designed to handle the uncertainty or disturbance introduced to the nominal system by the hysteresis effect. Adaptive neural control was developed in [24] and [25] for a class of nonlinear systems with PI-type input hysteresis. In [26], by using adaptive sliding mode control to online estimate the system parameters, position control of a piezoelectric stage was achieved without identifying or measuring the real values of the parameters of the stage. H_∞ robust feedback control combined with feedforward control based on system inversion was introduced [27] to achieve high-speed precision output tracking of a piezoelectric stage. A fuzzy decentralized control approach was proposed and applied for trajectory tracking of a 2-D piezo-driven system in [28].

The objective of this paper is to mitigate the hysteresis effect of the piezoelectric stage and achieve the desired tracking performance without the detailed hysteresis model except the slope

Manuscript received July 28, 2015; revised November 18, 2015 and January 9, 2016; accepted February 5, 2016. Date of publication March 15, 2016; date of current version September 9, 2016.

J. Chen and B. Ren are with the Department of Mechanical Engineering, Texas Tech University, Lubbock, TX 79409-1021 USA (e-mail: jinhao.chen@ttu.edu; beibei.ren@ttu.edu).

Q.-C. Zhong is with the Department of Electrical and Computer Engineering, Illinois Institute of Technology, Chicago, IL 60616 USA (e-mail: zhongqc@ieee.org).

Color versions of one or more of the figures in this paper are available online at http://ieeexplore.ieee.org.

Digital Object Identifier 10.1109/TIE.2016.2542780

information of the PI hysteresis asymptotes. However, unlike those aforementioned robust but complex controllers, a more simplified and robust alternative based on the uncertainty and disturbance estimator (UDE) will be developed in this paper. The UDE is constructed based on an assumption that any engineering signal can be recovered via a filter with the appropriate bandwidth [29]. Recently, the UDE-based controller was applied to a class of nonlinear nonaffine systems in [30], where the uncertainty and disturbance were well estimated and compensated. Motivated by [30], the extraordinary capability of the UDE-based controller will be explored in this paper to mitigate the hysteresis effects and fulfill some trajectory tracking tasks on a P-753.31c piezoelectric stage. Extensive experimental results using the PID controller and a disturbance-observer (DOB)-based controller [31]–[33] are provided for comparison.

This paper is organized as follows. The preliminaries and problem formulation are given in Section II. In Section III, the UDE-based controller will be designed for piezoelectric stages and the stability analysis of the closed-loop system will be provided. Experimental results are discussed in Section IV. Conclusion will be made in Section V.

II. Preliminaries of Hysteresis Model and Problem Formulation

A. Introduction of PI Hysteresis Model

As one of the basic hysteresis operators of PI model, the play operator F_r with threshold r can be defined for a given input $v(t) \in C_m[0,\ t_E]$ as [7]

$$\begin{aligned} F_r[v](0) &= f_r(v(0),\ 0) \\ F_r[v](t) &= f_r(v(t),\ F_r[v](t_i)) \\ f_r(v,\ w) &= \begin{cases} \max(v-r, w), & \text{for } v > v(t_i) \\ \min(v+r, w), & \text{for } v < v(t_i) \\ w, & \text{for } v = v(t_i) \end{cases} \\ &\text{for } t_i < t \le t_{i+1} \text{ and } 0 \le i \le N-1 \end{aligned} \tag{1}$$

where $0 = t_0 < t_1 < \cdots < t_N = t_E$ is partition of $[0,\ t_E]$, such that the function v is monotone on each of the subintervals $(t_i,\ t_{i+1}]$. The argument of the operator is written in square brackets to indicate the functional dependence, since it maps a function to a function. Such a play operator defined as (1) is shown in Fig. 1(a).

The PI hysteresis model $H[v](t)$ is then introduced through a weighted superposition of basic play operators $F_r[v](t)$ as follows [7]:

$$u(t) = H[v](t) = \int_0^R p(r) F_r[v](t) dr \tag{2}$$

where $u(t)$ is the hysteresis output, and $p(r)$ is an integrable density function, satisfying $p(r) \ge 0$ with $\int_0^\infty r p(r) dr < \infty$, and is expected to be identified from experimental data. When the density function is $p(r) = 0.12e^{-0.16r}$ with $r \in [0,\ 6]$ and $v(t) = 4.5\sin(0.75\pi t) + 3\sin(0.5\pi t)$, the plot of input $v(t)$ against output $u(t)$ of the PI model (2) is shown as the black solid line in Fig. 1(b).

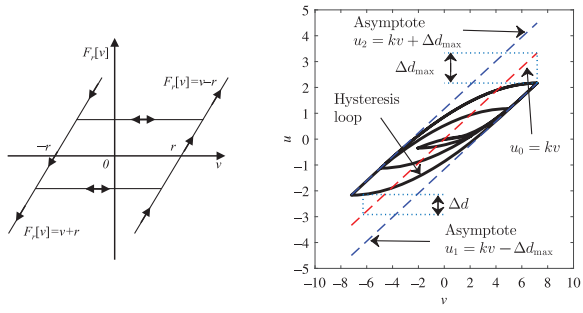

(a) (b)

Fig. 1. Illustration of PI hysteresis (2). (a) Play operator and (b) PI model and its asymptotes when $p(r) = 0.12e^{-0.16r}$ with $r \in [0,\ 6]$.

B. Asymptotes of PI Hysteresis Model

Fig. 1(b) shows that the PI hysteresis loop has a lower asymptote u_1 and an upper asymptote u_2. Due to the shape of the play operator in Fig. 1(a), the PI model (2) will converge to u_1 (or u_2) if and only if all operators $F_r[v](t)$ with different thresholds r are following their right (or left) slopes. Also, because of the symmetry of the play operator (1), these two asymptotes u_1 and u_2 are parallel. Furthermore, the PI hysteresis loop only exists within these two asymptotes. Thus, considering the line $u_0 = kv$ passing through the origin and parallel to u_1 and u_2, the PI model (2) can be rewritten as a linear term u_0 plus an unknown nonlinear term Δd, which will be used to facilitate the control design later

$$u(t) = kv(t) + \Delta d(t) \tag{3}$$

where $\Delta d(t) = H[v](t) - kv(t)$.

C. Problem Formulation

The linear dynamics of a piezoelectric stage can be identified as a second-order linear system as follows:

$$\ddot{y}(t) + 2\zeta\omega_n \dot{y}(t) + \omega_n^2 y(t) = \omega_n^2 u(t) + d_1(t) \tag{4}$$

where $y(t)$ is the system output (i.e., the stage displacement) and $u(t)$ is the excitation force generated by piezoelectric material deformation when the input voltage $v(t)$ is applied. Due to the hysteresis effect in the piezoelectric stage, the relationship between the excitation force $u(t)$ and the input voltage $v(t)$ is usually nonlinear and hysteretic, which will be characterized by the PI model (2) in this paper. $d_1(t)$ includes some unknown bounded disturbance and uncertainties (e.g., creep effect, parametric variability of input hysteresis, and system dynamics modeling error).

Define $x(t) = [\,x_1(t)\ x_2(t)\,]^T = [\,y(t)\ \dot{y}(t)\,]^T$ as the state vector, then (4) can be re-expressed as

$$\begin{aligned} \begin{bmatrix} \dot{x}_1(t) \\ \dot{x}_2(t) \end{bmatrix} &= \begin{bmatrix} 0 & 1 \\ -\omega_n^2 & -2\zeta\omega_n \end{bmatrix} \begin{bmatrix} x_1(t) \\ x_2(t) \end{bmatrix} \\ &+ \begin{bmatrix} 0 \\ \omega_n^2 \end{bmatrix} u(t) + \begin{bmatrix} 0 \\ d_1(t) \end{bmatrix}. \end{aligned} \tag{5}$$

Substituting the input hysteresis (2) into (5), the full dynamics model of the piezoelectric stage can be obtained as

$$\dot{x}(t) = Ax(t) + BH[v](t) + d(t) \tag{6}$$

with $A = [\,0\ 1;\ -\omega_n^2\ -2\zeta\omega_n\,]$ and $B = [\,0\ \omega_n^2\,]^T$, $d(t) = [\,0\ \ d_1(t)\,]^T$.

In order for the closed-loop system to meet the required specifications, the following stable reference model (RM) in a controllable canonical form can be chosen:

$$\dot{x}_m(t) = A_m x_m(t) + B_m c(t) \tag{7}$$

where $x_m(t) = [\,y_m(t)\ \dot{y}_m(t)\,]^T$ is the reference state vector and $c(t)$ is a piecewise continuous and uniformly bounded command to this reference system with $A_m = [\,0\ 1;\ -a_{m1}\ -a_{m2}\,]$ and $B_m = [\,0\ b_m\,]^T$. The control objective is to design the input to the hysteresis unit or the control signal $v(t)$ so that the tracking error $e(t) = [\,e_1(t)\ e_2(t)\,]^T = x_m(t) - x(t)$ asymptotically converges to zero with the desired error dynamics governed by

$$\dot{e}(t) = (A_m + K)e(t) \tag{8}$$

where the error feedback gain matrix is in the form of $K = [\,0\ 0;\ -K_{21}\ -K_{22}\,]$.

III. Control Design and Stability Analysis

A. UDE-Based Controller Design

The UDE-based controller will be designed in this section for the tracking problem stated in Section II-C. To facilitate the control design, the dynamics model of piezoelectric stage (6) is reformulated as

$$\begin{aligned}\dot{x}(t) &= Ax(t) + B\cdot[kv(t) + H[v](t) - kv(t)] + d(t)\\ &= Ax(t) + B\cdot kv(t) + u_d(v(t))\end{aligned} \tag{9}$$

where k is the input gain from (3), the lumped vector $u_d(v(t)) = [0\ u_{d2}(t)]^T$ includes the PI hysteresis $H[v](t)$, the control signal $v(t)$ and the disturbance and uncertainties term $d(t)$, i.e.,

$$u_d(v(t)) := B\cdot[H[v](t) - kv(t)] + d(t). \tag{10}$$

By combining (7)–(9), the control signal $v(t)$ should satisfy

$$Bkv(t) = A_m x(t) + B_m c(t) - Ax(t) - u_d(v(t)) - Ke(t). \tag{11}$$

According to the system dynamics (9), the lumped uncertainty and disturbance term $u_d(v(t))$ can be represented as

$$u_d(v(t)) = \dot{x}(t) - Ax(t) - Bkv(t). \tag{12}$$

This shows that the lumped term can be obtained from the known dynamics of the piezoelectric stage and voltage input. However, the direct use of this relation will cause algebraic loops and the control law cannot be formulated. In [29], this signal was estimated by a filter in the frequency domain. This is achievable because a signal can be recovered by a filter of which the bandwidth is wide enough to cover the spectrum of that signal. According to the assumption in [29], if a stable filter $G_f(s)$ is strictly proper and has the unity gain and zero phase shift over the spectrum of $u_d(v(t))$ and zero gain elsewhere, then $u_d(v(t))$ can be accurately estimated as

$$\begin{aligned}\hat{u}_d(v(t)) &= u_d(v(t)) * g_f(t)\\ &= (\dot{x}(t) - Ax(t) - Bkv(t)) * g_f(t)\end{aligned} \tag{13}$$

where "$*$" is the convolution operator and $g_f(t)$ is the impulse response of $G_f(s)$. This procedure is equivalent to amplifying the signal $u_d(v(t))$ by the gain 1 without shifting the phase for the frequency components that fall into the bandwidth of the filter $G_f(s)$, and at the same time, blocking anything outside the bandwidth of the filter $G_f(s)$, which is 0 anyway. Therefore, the signal is well represented without adding or losing any information. Replacing $u_d(v(t))$ in (11) with $\hat{u}_d(v(t))$ in (13) results in

$$\begin{aligned}Bkv(t) = {} & A_m x(t) + B_m c(t) - Ax(t) - Ke(t)\\ & -(\dot{x}(t) - Ax(t) - Bkv(t)) * g_f(t).\end{aligned} \tag{14}$$

By denoting $Bkv(t) = \phi(t)$, there is

$$\begin{aligned}\phi(t) = {} & (A_m x(t) + B_m c(t) - Ke(t)) * \mathcal{L}^{-1}\left\{\frac{1}{1 - G_f(s)}\right\}\\ & -Ax(t) - x(t) * \mathcal{L}^{-1}\left\{\frac{sG_f(s)}{1 - G_f(s)}\right\}\end{aligned} \tag{15}$$

where $\mathcal{L}^{-1}\{\cdot\}$ is the operator of inverse Laplace transform.

Noting that (6) and (7), (15) can be rewritten as

$$\begin{aligned}\begin{bmatrix}0\\ \omega_n^2\end{bmatrix} kv(t) &= \phi(t)\\ &= \mathcal{L}^{-1}\left\{\frac{1}{1 - G_f(s)}\right\} * \left(\begin{bmatrix}0 & 1\\ -a_{m1} & -a_{m2}\end{bmatrix}\begin{bmatrix}y(t)\\ \dot{y}(t)\end{bmatrix}\right.\\ &\quad \left. + \begin{bmatrix}0\\ b_m\end{bmatrix} c(t) - \begin{bmatrix}0 & 0\\ -K_{21} & -K_{22}\end{bmatrix}\begin{bmatrix}e_1(t)\\ e_2(t)\end{bmatrix}\right)\\ &\quad - \begin{bmatrix}0 & 1\\ -\omega_n^2 & -2\zeta\omega_n\end{bmatrix}\begin{bmatrix}y(t)\\ \dot{y}(t)\end{bmatrix}\\ &\quad - \begin{bmatrix}y(t)\\ \dot{y}(t)\end{bmatrix} * \mathcal{L}^{-1}\left\{\frac{sG_f(s)}{1 - G_f(s)}\right\}\end{aligned} \tag{16}$$

it can be found that the first equation is always satisfied (zero on both sides). That means the solution for the second equation [i.e., $\omega_n^2 \cdot kv(t) = [\,0\ 1\,]\,\phi(t)$], which is uniquely solved as $v(t) = [\,0\ 1/\omega_n^2\,]\,\phi(t)/k$, can be used as the controller to fulfill the trajectory tracking task. Denoting the pseudo-inverse of B as B^+, which can be calculated as $B^+ = (B^TB)^{-1}B^T = [\,0\ 1/\omega_n^2\,]$, the UDE-based controller for the piezoelectric stage is then established as follows:

$$v(t) = \frac{1}{k}B^+\phi(t). \tag{17}$$

B. Stability Analysis

The following lemma shows the boundedness of Δd in (3), which will be used in the stability analysis of the UDE-based controller.

Lemma 1. For the PI hysteresis (2), it can be reconstructed as $u(t) = kv(t) + \Delta d(t)$, where $\Delta d(t) = H[v](t) - kv(t)$ is always bounded if $k = \int_0^R p(r)dr$.

Proof: According to (1), if $\dot{v}(t) > 0$, i.e., $v(t) > v(t_i)$, there is $f_r(v,\ w) = \max(v - r, w) \geq v - r$. Therefore, $F_r[v](t) \geq v(t) - r$. Then, from (2)

$$\begin{aligned} u(t) &= \int_0^R p(r)F_r[v](t)dr \\ &\geq \int_0^R p(r)(v(t) - r)dr \\ &= v(t)\int_0^R p(r)dr - \int_0^R p(r)rdr. \end{aligned}$$

The equality occurs only when $F_r[v](t) = v(t) - r$, and this will be satisfied afterward until $\dot{v}(t) < 0$. That is, for $\dot{v}(t) > 0$, the PI hysteresis will converge to the lower asymptote defined as $u_1(t) := v(t)\int_0^R p(r)dr - \int_0^R p(r)rdr$. Since the density function satisfies $p(r) \geq 0$ with $\int_0^\infty rp(r)dr < \infty$, there exists a constant $\Delta d_{\max} = \int_0^R p(r)rdr$. By letting $k = \int_0^R p(r)dr$, the lower asymptote becomes $u_1(t) := kv(t) - \Delta d_{\max}$ and

$$u(t) - kv(t) \geq -\Delta d_{\max}. \tag{18}$$

Similarly, for $\dot{v}(t) < 0$, i.e., $v(t) < v(t_i)$, there is $F_r[v](t) \leq v(t) + r$, and thus

$$u(t) \leq u_2(t) := kv(t) + \int_0^R p(r)rdr.$$

Then, it can be obtained that

$$u(t) - kv(t) \leq \Delta d_{\max}. \tag{19}$$

By combining (18) and (19) and defining $\Delta d(t) = u(t) - kv(t)$, there is

$$|\Delta d(t)| \leq \Delta d_{\max}.$$

This completes the proof. ■

As an example for Lemma 1, the slope of the asymptotes for the PI hysteresis shown in Fig. 1(b) can be calculated by $k = \int_0^6 0.12e^{-0.16r}dr = 0.4628$. Also, the bound of nonlinear term $\Delta d(t)$ is obtained as $\Delta d_{\max} = \int_0^6 r0.12e^{-0.16r}dr = 1.1697$.

Theorem 2. The closed-loop system consisting of the plant (6) preceded by input hysteresis characterized by the PI model (2), the RM (7), and the controller (17), is asymptotically stable, if 1) the filter $G_f(s)$ in (16) is strictly proper and stable with $G_f(0) = 1$; 2) the disturbance $d(t)$ is bounded; and 3) the input gain k in (17) is chosen properly as $k = \int_0^R p(r)dr$, where $p(r)$ is the density function of PI hysteresis model (2).

Proof: By substituting the control law (17), which takes into account the estimation of $u_d(v(t))$ as in (13), into (9) and taking the Laplace transform, there is

$$sX(s) = AX(s) + U_d(s) + BB^+\Phi(s). \tag{20}$$

The Laplace transform of the reference system (7) is

$$sX_m(s) = A_mX_m(s) + B_mC(s). \tag{21}$$

According to (12) and (14), the Laplace transform of $\phi(t)$ becomes

$$\begin{aligned} \Phi(s) = A_mX(s) + B_mC(s) - AX(s) - KE(s) \\ -U_d(s)G_f(s) \end{aligned} \tag{22}$$

where $U_d(s)$ is the Laplace transform of $u_d(v(t))$. Combining (20)–(22) results in

$$\begin{aligned} sE(s) =& sX_m(s) - sX(s) \\ =& (A_m + K)E(s) - U_d(s)[1 - G_f(s)] \\ &+ (I - BB^+)\Phi(s). \end{aligned}$$

Since $BB^+ = [0\ 0;\ 0\ 1]$ and the first element of $\phi(t)$ is 0, there is $(I - BB^+)\phi(t) = 0$. Then, the actual error dynamics of the closed-loop system is

$$E(s) = -[sI - (A_m + K)]^{-1}U_d(s)[1 - G_f(s)]. \tag{23}$$

According to Lemma 1, $H[v](t) - kv(t)$ is bounded if $k = \int_0^R p(r)dr$. Since $d(t)$ is assumed to be bounded, $u_d(v(t)) = B\cdot[H[v]\cdot(t) - kv(t)] + d(t)$ is also bounded, which means $\lim_{s\to 0} sU_d(s)$ is bounded. Moreover, as aforementioned, $G_f(s)$ is strictly proper and stable with $G_f(0) = 1$ and $[sI - (A_m + K)]^{-1}$ is stable by design, so the error dynamics is stable. Therefore, by applying the final value theorem to (23),

$$\begin{aligned} \lim_{t\to\infty} e(t) &= \lim_{s\to 0} s \cdot E(s) \\ &= \lim_{s\to 0} -[sI - (A_m + K)]^{-1} \cdot sU_d(s) \cdot [1 - G_f(s)] \\ &= 0 \end{aligned}$$

which means that $x(t)$ asymptotically track the reference states $x_m(t)$. This completes the proof. ■

IV. Experimental Validation

A. Experimental Setup

To validate the effectiveness of the proposed UDE-based controller, a set of experiments have been conducted on a Physik Instrumente P-753.31c piezoelectric nanopositioning stage with high resolution capacitive position sensor (see Fig. 2). In this setup, a host computer sends the control signal $v(t)$ through dSPACE-DS1104 to E-505.00 linear voltage amplifier with a fixed gain of 10, and finally actuates the P-753.31c piezoelectric stage of which the maximum displacement is 38 μm from its static equilibrium point. The displacement of the piezoelectric stage is obtained by E-509.C1A sensor monitor from an integrated capacitive sensor (sensitivity = 3.8 μm/V; resolution = 0.2 nm). The detailed specification of the piezoelectric nanopositioning system is listed in Table I. The output voltage of E-509.C1A is then sampled by dSPACE-DS1104 at a sampling frequency of 20 kHz.

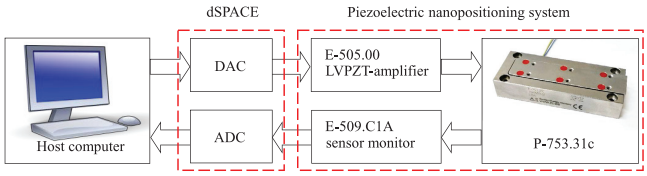

Fig. 2. Experimental setup of Physik Instrumente P-753.31c piezoelectric nanopositioning system.

TABLE I
PARAMETERS OF THE PIEZOELECTRIC NANOPOSITIONING SYSTEM USED IN EXPERIMENTS

Module	Parameter	Value[a]	Unit
E-505.00	Control input	–2 to 12	V
	DC-offset to control input	0 to 10	V
	Voltage gain	10±0.1	–
	Output voltage	–30 to 130	V
P-753.31c	Mass	250	g
	Nominal expansion	38	µm
	Unloaded resonant frequency	2.9±20%	kHz
	Stiffness in motion direction	16±20%	N/µm
	Full-range repeatability	±3	nm
E-509.C1A	Output	0 to 10	V
	Sensitivity	3.8	µm/V
	Resolution	0.2	nm
	Bandwidth	3	kHz
	Linearity (typ.)	0.05%	–

a Cited from http://www.pi.ws

B. System Identification

1) Hysteresis Modeling: Instead of having the input gain $k = \int_0^R p(r)dr$ to ensure the asymptotic stability of the closed-loop system as shown in Theorem 2, it will be shown in the experimental results that k can be obtained from the observation of the measured hysteresis loop. Therefore, in order to verify 1) the existence of the PI hysteresis in the P-753.31c piezoelectric stage and 2) the accuracy of the estimated slope of hysteresis asymptotes, the hysteresis model of the P-753.31c piezoelectric stage is identified. To this end, an input signal to the piezoelectric stage is set to be a triangular signal with the frequency 1 Hz and the magnitude 6 V as shown in Fig. 3(a). In this paper, the form of the density function $p(r)$ in the PI model (2) is specified as

$$p(r_i) = \rho e^{-\lambda r_i}$$

and the threshold values r_i are directly given by

$$r_i = \frac{i}{j}||v(t)||_\infty, \quad i = 0,\ 1,\ 2, \ldots,\ j-1.$$

Since $||v(t)||_\infty = \max\{|v(t)|\} = 6$, we can have $r_i = 0.1i$, $i = 0,\ 1,\ 2, \ldots,\ j-1$ by setting $j = 60$. The identification of hysteresis models is quite challenging, but it is not the focus of this paper. Interested readers can refer to the least square method [34] and particle swarm optimization [35]. By using the least square method, the density function is identified as $p(r_i) = 9.0616e^{-2.2273r_i}$. The comparison between the identified PI model and the experimental data of the piezoelectric stage is presented in Fig. 3(b). The slope of the asymptotes can be then calculated as $k = 4.5383$.

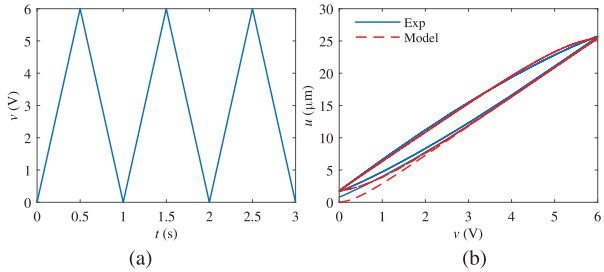

Fig. 3. Hysteresis modeling result. (a) Hysteresis input $v(t)$. (b) Hysteresis loop.

2) System Modeling: To identify the linear part of the system model of the piezoelectric stage

$$\frac{Y(s)}{U(s)} = \frac{\omega_n^2}{s^2 + 2\zeta\omega_n s + \omega_n^2}$$

the excitation force $u(t)$ is obtained by $H[v](t)$. By collecting and analyzing the step response of the piezoelectric system, the overshoot percentage and peak time are found as $M_p = 1.54\%$, and $t_p = 0.0065\,\mathrm{s}$, respectively. Then, the natural frequency and damping ratio are calculated as $\omega_n = 804.0072\,\mathrm{rad/s}$ and $\zeta = 0.7991$. Thus, the system dynamics of the P-753.31c piezoelectric stage is identified as

$$\dot{x}(t) = \begin{bmatrix} 0 & 1 \\ -646430 & -1285 \end{bmatrix} x(t) + \begin{bmatrix} 0 \\ 646430 \end{bmatrix} u(t) \tag{24}$$

where $u(t) = H[v](t)$ is the PI hysteresis output fed by the control signal $v(t)$.

C. Control Design

As noted in Theorem 2, the filter $G_f(s)$ should be strictly proper and stable with $G_f(0) = 1$ to achieve the asymptotic stability of the closed-loop system. The following first-order low-pass filter is considered in practice:

$$G_f(s) = \frac{1}{1+\tau s} \tag{25}$$

with the time constant τ. For nonstep reference signals, the UDE-based controller with such a filter would lead to a nonzero but small estimation error $\tilde{u}_d(v(t)) = u_d(v(t)) * [1 - g_f(t)]$ and thus degraded performance. However, the performance could still be excellent when a small enough τ is chosen so that the bandwidth of the filter (25) is wide enough to cover most spectrum of $u_d(v(t))$. The impact of different choices of τ on the tracking performance will be investigated later.

Using such a filter (25), the UDE-based controller from (17) can be further derived as

$$\begin{aligned} v(t) = &\frac{1}{k\omega_n^2}\Big[\,(-a_{m1}y(t) - a_{m2}\dot{y}(t) + b_m c(t) + K_{21}e_1(t) \\ &+ K_{22}e_2(t) + \omega_n^2 y(t) + 2\zeta\omega_n\dot{y}(t)) - \frac{1}{\tau}\dot{y}(t) \\ &+ \frac{1}{\tau}\int_0^t (-a_{m1}y(\xi) - a_{m2}\dot{y}(\xi) + b_m c(\xi) \\ &+ K_{21}e_1(\xi) + K_{22}e_2(\xi))d\xi\,\Big]. \end{aligned} \tag{26}$$

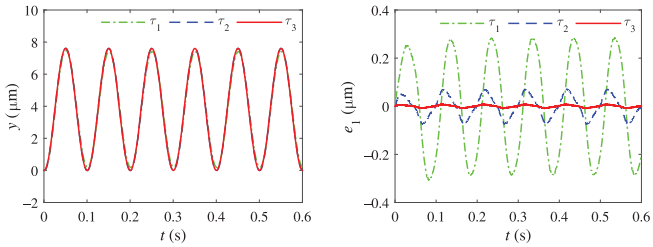

Fig. 4. Impact of different filter constants τ with $\tau_1 = 0.03\,\text{s}$, $\tau_2 = 0.003\,\text{s}$, and $\tau_3 = 0.0003\,\text{s}$ with $A_m + K = [\,0\;\;1;\;-1400^2\;\;-336\,]$ and $k = 26/6$. (a) Position $y(t)$. (b) Tracking error $e_1(t)$.

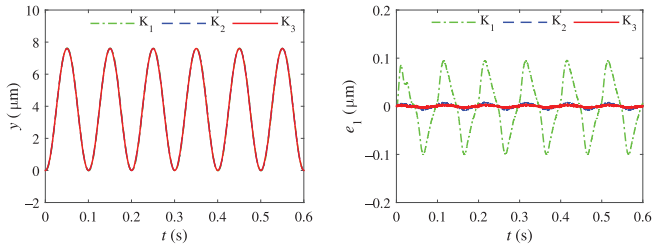

Fig. 5. Impact of different error feedback gains K such that $A_m + K_1 = [\,0\;\;1;\;-400^2\;\;-96\,]$, $A_m + K_2 = [\,0\;\;1;\;-1400^2\;\;-336\,]$ and $A_m + K_3 = [\,0\;\;1;\;-2400^2\;\;-576\,]$ with $k = 26/6$ and $\tau = 0.0003\,\text{s}$. (a) Position $y(t)$. (b) Tracking error $e_1(t)$.

D. Guidelines for Selecting Control Parameters

In this section, the guidelines for selecting parameters in the UDE-based controller (26) will be discussed. In order to have the bandwidth of the closed-loop system higher than 100 Hz, which is generally required in industrial applications [36], the RM is chosen as

$$\dot{x}_m(t) = \begin{bmatrix} 0 & 1 \\ -6000^2 & -12000 \end{bmatrix} x_m(t) + \begin{bmatrix} 0 \\ 6000^2 \end{bmatrix} c(t) \quad (27)$$

with the input signal $c(t)$ set to be $c(t) = 3.8 + 3.8\sin(2\pi f t - \pi/2)$ (μm). The initial states of the system are set to be $x(0) = [\,0\;\;0\,]^T$.

1) Effect of Input Gain k: Theoretically, according to Lemma 1, when input gain k is chosen as the slope of asymptotes of PI model (2), i.e., $k = \int_0^R p(r)dr$, $\Delta d(t) = H[v](t) - kv(t)$ is bounded by $\Delta d_{\max} = \int_0^R p(r)r dr$, which guarantees the stability of the closed-loop system as mentioned in Theorem 2. In practice, instead of identifying the density function $p(r)$ and using $k = \int_0^R p(r)dr$, k can be approximated by the ratio of the output range and the corresponding input range directly from the hysteresis loop. Therefore, the detailed hysteresis model is not needed for the implementation of the UDE-based controller. From Fig. 3, it can be found that the ratio of the output range and the input range is about 26/6, which is very close to the slope of the asymptotes calculated from the identified density function, i.e., $k = 4.5383$. Thus, $k = 26/6$ is adopted in the following cases.

2) Effect of Filter Time Constant τ: With $k = 26/6$ and $A_m + K = [\,0\;\;1;\;-1400^2\;\;-336\,]$, three time constants $\tau_1 = 0.03\,\text{s}$, $\tau_2 = 0.003\,\text{s}$, and $\tau_3 = 0.0003\,\text{s}$ are tested with the results shown in Fig. 4. As aforementioned, better tracking performance should be achieved by using smaller value of τ, which can be verified from Fig. 4 that the case with $\tau_3 = 0.0003\,\text{s}$ achieves best performance among these three cases. In [37], some guidance of the filter design was provided by revealing the two-degree-of-freedom nature of the UDE-based controller. In practice, due to the limitations of sampling time, τ cannot be chosen too small. Also, the filter with too wide bandwidth, for τ being too small, will introduce sensor noise with high frequency, and thus might degrade the performance of the UDE-based controller. Therefore, how to choose τ depends on the specific application including the hardware capability and the performance requirements.

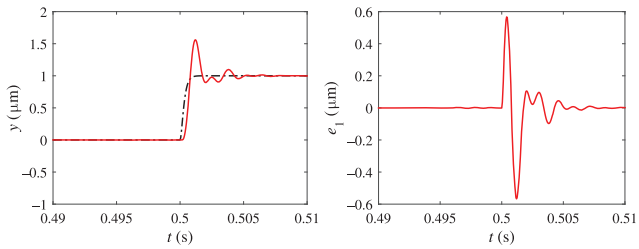

Fig. 6. Asymptotic tracking of a step signal. (a) Zoomed-in position $y(t)$. (b) Zoomed-in tracking error $e_1(t)$.

3) Effect of Error Feedback Gain K: Using $k = 26/6$ and $\tau = 0.0003\,\text{s}$, three error feedback gains K_1, K_2, and K_3 are chosen such that $A_m + K_1 = [\,0\;\;1;\;-400^2\;\;-96\,]$, $A_m + K_2 = [\,0\;\;1;\;-1400^2\;\;-336\,]$, and $A_m + K_3 = [\,0\;\;1;\;-2400^2\;\;-576\,]$, for which the results are shown in Fig. 5. It can be found that the tracking error is relatively small for $A_m + K_3 = [\,0\;\;1;\;-2400^2\;\;-576\,]$. This is because the real part of the eigenvalues of $A_m + K$ will determine the rate of convergence of the tracking error. Since the real parts of eigenvalues for $A_m + K_1$, $A_m + K_2$, and $A_m + K_3$ are -48, -168, and -288, respectively, it can be easily concluded that $A_m + K_3$ should have the faster rate of convergence of the tracking error, and it will have relatively smaller tracking error in practice.

E. Tracking Performance with Different Trajectories

Enlightened by Section IV-D, $k = 26/6$ and $A_m + K = [0\;1; -2400^2\;\;-576]$, $\tau = 0.0003\,\text{s}$ will be used for the UDE-based controller.

1) Tracking of a Step Signal: According to Theorem 2, the asymptotic stability of the closed-loop system can be achieved when $G_f(s)$ is strictly proper and stable with $G_f(0) = 1$. The filter $G_f(s)$ given in (25) satisfies this condition. To demonstrate the asymptotic stability of the UDE-based controller, the reference input $c(t)$ is set as a step signal with magnitude $1\,\mu\text{m}$ starting at $t = 0.5\,\text{s}$. The tracking results are shown in Fig. 6. It can be seen that the output of the closed-loop system can indeed asymptotically track the step signal and the settling time is about 5 ms.

2) Tracking of Sinusoidal Signals with Different Frequencies: The experimental results when the frequency

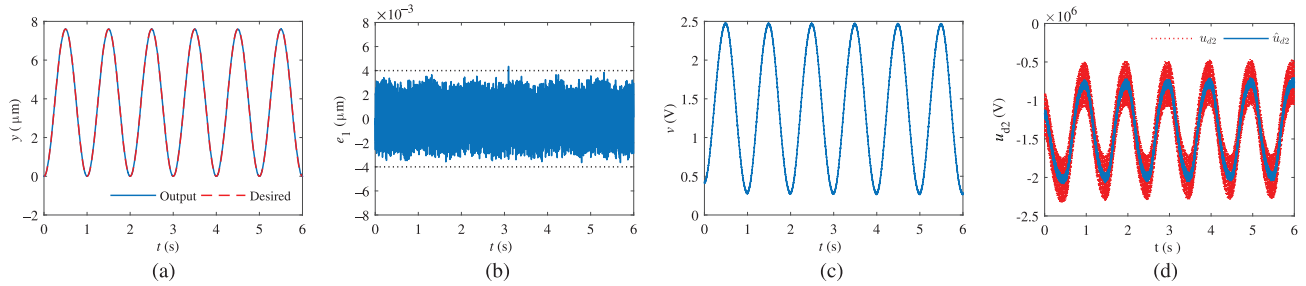

Fig. 7. 1-Hz sinusoidal trajectory tracking performance of a piezoelectric stage using the UDE-based controller. (a) Position $y(t)$. (b) Tracking error $e_1(t)$. (c) Control signal $v(t)$. (d) Uncertainty $u_{d2}(t)$ and its estimation $\hat{u}_{d2}(t)$.

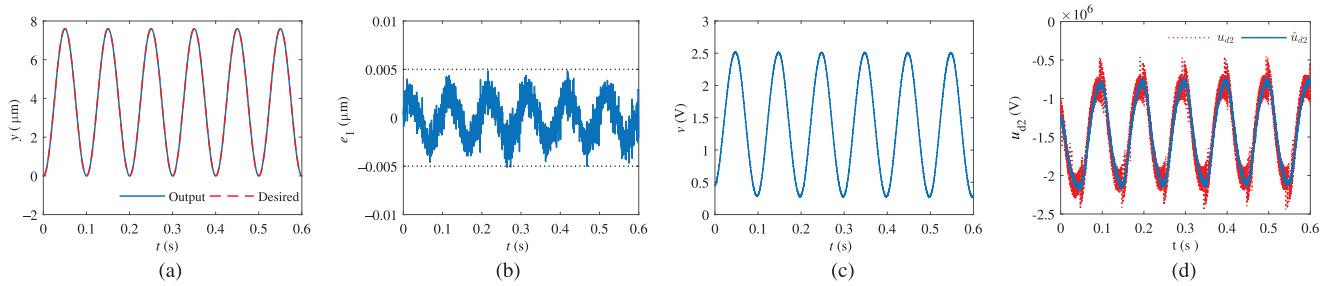

Fig. 8. 10-Hz sinusoidal trajectory tracking performance of a piezoelectric stage using the UDE-based controller. (a) Position $y(t)$. (b) Tracking error $e_1(t)$. (c) Control signal $v(t)$. (d) Uncertainty $u_{d2}(t)$ and its estimation $\hat{u}_{d2}(t)$.

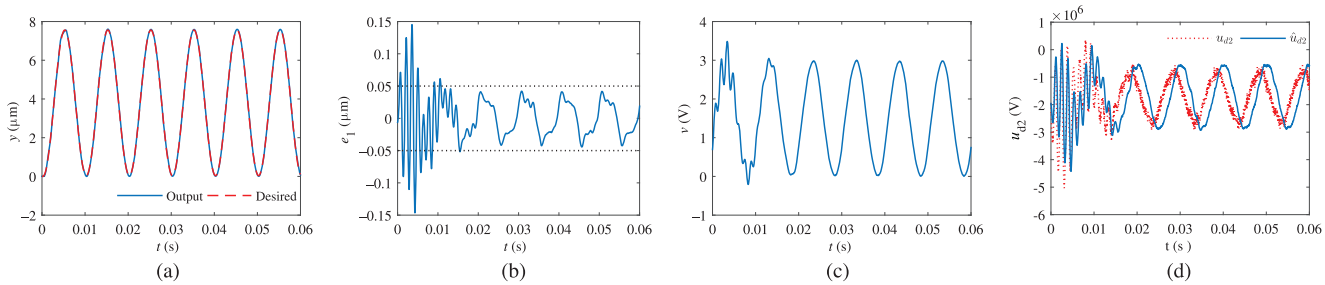

Fig. 9. 100-Hz sinusoidal trajectory tracking performance of a piezoelectric stage using the UDE-based controller. (a) Position $y(t)$. (b) Tracking error $e_1(t)$. (c) Control signal $v(t)$. (d) Uncertainty $u_{d2}(t)$ and its estimation $\hat{u}_{d2}(t)$.

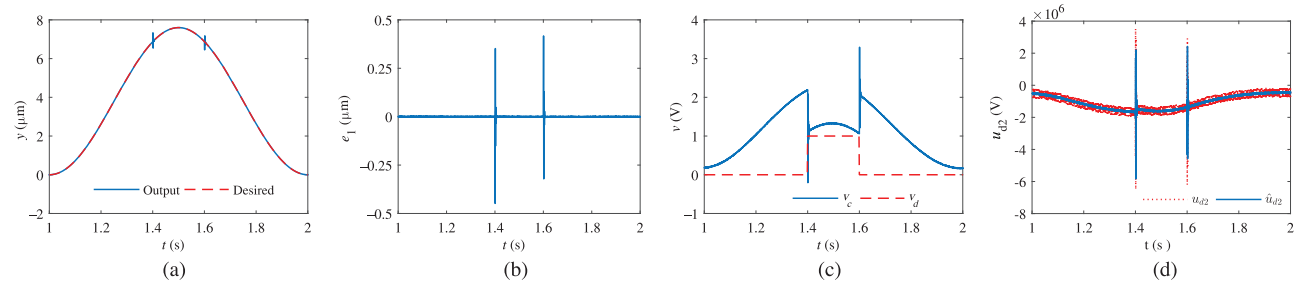

Fig. 10. 1-Hz sinusoidal trajectory tracking performance of a piezoelectric stage with input disturbance using the UDE-based controller. (a) Position $y(t)$. (b) Tracking error $e_1(t)$. (c) Control output signal $v_c(t)$ and input disturbance $v_d(t)$. (d) Uncertainty $u_{d2}(t)$ and its estimation $\hat{u}_{d2}(t)$.

f of the input signal $c(t)$ in the reference system (27) is set as 1, 10, and 100 Hz are shown in Figs. 7–9, respectively. It can be seen that each of the tracking tasks is well achieved by the UDE-based controller and the tracking errors are all relatively small. For $f = 100$ Hz, there exist oscillations during the transient state, which only lasts for about two periods, i.e., 20 ms, then the closed-loop system stays stable and its output well tracks the desired trajectory. Moreover, from Figs. 7(d), 8(d), and 9(d), it can be seen that UDE well estimates the uncertainty and disturbance lumped term $u_{d2}(t)$ as $\hat{u}_{d2}(t)$, which guarantees the performance of the UDE-based controller.

3) With an Additive Input Disturbance: In this part, a disturbance $v_d = 1$ V is directly added to the control input between $t_{\text{begin}} = 1.4$ s and $t_{\text{end}} = 1.6$ s as shown in Fig. 10(c). The system input is calculated as $v = v_c + v_d$ with v_c as the control output obtained by the UDE-based controller, and the reference input is set to be $c(t) = 3.8 + 3.8\sin(2\pi t - \pi/2)$ (μm). The results are shown in Fig. 10. It can be seen

that there exist oscillations near t_{begin} and t_{end} as observed from Fig. 10(b), which only lasts for less than 10 ms. This well demonstrates the robustness of the UDE-based controller. From Fig. 10(d), it can be found that the uncertainty and disturbance u_{d2} is changed due to the add-in disturbance v_d. However, this change is captured and compensated by the proposed UDE-based controller, which results in the change in v_c shown in Fig. 10(c). This ensures the effectiveness and robustness of the UDE-based controller.

F. Comparison With Other Controllers

In this section, two other well-tuned controllers, namely the PID controller and a DOB-based controller, will be considered with extensive experimental results presented for the purpose of comparison. For the PID controller, the parameters are tuned as $K_{p1} = 0.2381$, $K_{i1} = 238.08$, and $K_{d1} = 5.9520 \times 10^{-5}$. The derivative of the trajectory signal, i.e., the speed signal $\dot{y}$, is used to obtain $\dot{e}_1$ because $\dot{y}_m$ is available from the RM. The DOB-based controller takes the one proposed in [33] with the following second-order Butterworth filter:

$$Q(s) = \frac{1}{(\tau_Q s)^2 + \sqrt{2}\tau_Q s + 1}$$

with $\tau_Q = 1/1000$ s. P_N^{-1} is constructed based on the identified system (24) and K_N is chosen in the same way as k, i.e., $K_N = 26/6$. A PID controller is introduced for $C(s)$ with the parameters carefully tuned as $K_{p2} = 1.3$, $K_{i2} = 830$, and $K_{d2} = 0$.

It should be noted that both UDE- and DOB-based controllers adopt filters, which satisfy $G_f(0) = 1$ and $Q(0) = 1$, respectively. However, these filters play different roles. In the UDE-based controller, the adoption of $G_f(s)$ is to approximate a signal based on an assumption mentioned in [29], while the purpose of adding a filter $Q(s)$ in DOB is to make $Q(s)P_N^{-1}$ proper and implementable. Therefore, $G_f(s)$ in UDE can generally be any proper filter with an arbitrary positive relative degree, while $Q(s)$ in DOB must have at least the same relative degree as P_N. This explains why, in this case, a second-order or even higher order filter is needed for $Q(s)$ while even a first-order filter can be used for $G_f(s)$.

1) Tracking Errors for Sinusoidal Signals With Different Frequencies: For sinusoidal signals with frequencies 1, 10, 50, and 100 Hz, Table II summarizes the steady-state tracking errors in terms of root-mean-squared error E_{rms}, maximum absolute error E_{m}, and relative maximum absolute error E_{rm} of the UDE-based, the DOB-based, and the PID controllers. These are calculated as follows:

$$E_{\text{rms}} = \sqrt{\frac{1}{N}\sum_{n=1}^{N}(y_m(t_n) - y(t_n))^2}$$

$$E_{\text{m}} = \max_{n\in[1,N]} |y_m(t_n) - y(t_n)|$$

$$E_{\text{rm}} = \frac{E_m}{\max_{n\in[1,N]} |y_m(t_n)|} \times 100\%$$

where N is the total number of data collected, $y_m(t_n)$ and $y(t_n)$ are the desired output and the system output at $t = t_n$,

TABLE II
ERRORS IN DIFFERENT TRAJECTORY TRACKING TASKS BY USING DIFFERENT CONTROLLERS

f (Hz)	Controller	E_{rms} (μm)	E_{m} (μm)	E_{rm} (%)
1	UDE	0.0012	0.0044	0.06
	DOB	0.0049	0.0107	0.14
	PID	0.0207	0.0423	0.56
10	UDE	0.0019	0.0051	0.07
	DOB	0.0465	0.0680	0.89
	PID	0.2010	0.2965	3.90
50	UDE	0.0103	0.0194	0.26
	DOB	0.2266	0.3138	4.13
	PID	0.2010	0.2965	3.90
100	UDE	0.0256	0.0444	0.58
	DOB	0.5768	0.8725	11.48
	PID	1.1254	1.6120	21.21

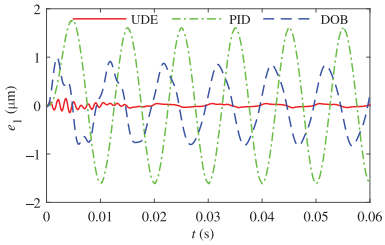

Fig. 11. Tracking error obtained from the UDE-based controller, the PID controller, and the DOB-based controller for a 100-Hz sinusoidal signal.

respectively. Note that the values in Table II are calculated with data points in the steady state within three periods, i.e., $t_N - t_1 = 3/f$ s. From Table II, it can be concluded that the performance of the UDE-based controller is much better than the other two controllers. For example, when $f = 1$ Hz, in term of E_{rms}, the UDE-based controller achieves less than $1/4$ of the DOB-based controller, and less than 1/17 of the PID controller. In terms of E_{m} or E_{rm}, the UDE-based controller achieves about $2/5$ of the DOB-based controller and 1/10 of the PID controller. Similar conclusions can be drawn from the cases with $f = 10$, 50, or 100 Hz that the UDE-based controller achieves much smaller tracking errors compared to the PID and DOB-based controllers in terms of E_{rms}, E_{m}, and E_{rm}. In order to demonstrate this more clearly, the tracking errors from the three controllers for $f = 100$ Hz are shown in Fig. 11. Indeed, the tracking error of the UDE-based controller is much smaller than those of the other two controllers.

2) Bandwidth of the Open-Loop System and the Closed-Loop System: To further show the effectiveness and robustness of the UDE-based controller, the frequency responses of the open-loop system and the closed-loop systems using the UDE-based controller and the DOB-based controller are tested and shown in Fig. 12. It is observed that the bandwidth of the open-loop system (i.e., the first time that the magnitude drops 3 dB) is about 100 Hz, and the behavior of the open-loop system is quite different from that of the RM. For the closed-loop system with the UDE-based controller, it can track the reference signal well up to 450 Hz, which is much broader than the desired bandwidth 100 Hz mentioned in [36], while the closed-loop system with the DOB-based controller can only track the reference signal up to 200 Hz. It is worth noting that, in the frequency response of the closed-loop systems,

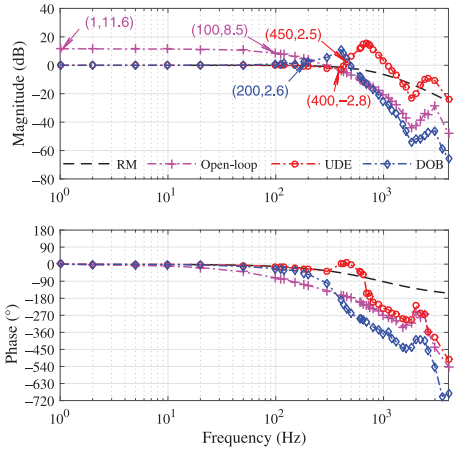

Fig. 12. Bode plots of the open-loop system, the closed-loop systems, and the RM.

there is an additional resonant peak at around 700 and 400 Hz, respectively, which is introduced by the controller, in addition to the resonant peak at around 3 kHz from the open-loop system as can be seen from Fig. 12 and Table I. However, the additional resonant peak in either case is not a problem because the resonant frequency is much higher than the desired bandwidth 100 Hz required in industry.

V. Conclusion

In this paper, the dynamics model of the piezoelectric stage has been identified as a second-order linear system preceded by the hysteresis characterized by the PI model. The UDE-based controller has been developed and applied to the piezoelectric stage positioning control with guidelines given for tuning the control parameters. It has been theoretically and experimentally shown that the hysteresis nonlinearity and other unknown bounded uncertainties, e.g., creep, modeling error, and external unknown input disturbance, in P-753.31c piezoelectric stage can be well compensated by the UDE-based controller and the overall closed-loop system can achieve asymptotic stability. Compared to the PID controller and the DOB-based controller, the UDE-based controller has achieved much better tracking performance. Also, the closed-loop system with the UDE-based controller can track the reference signal well in a broader frequency range compared to that with the DOB-based controller. The effectiveness and robustness of the UDE-based controller has been well verified and demonstrated.

Acknowledgment

The authors would like to thank the reviewers and the editors for their constructive comments and suggestions, which have helped enhance the presentation of this paper.

References

[1] J.-W. Wu, K.-C. Huang, M.-L. Chiang, M.-Y. Chen, and L.-C. Fu, "Modeling and controller design of a precision hybrid scanner for application in large measurement-range atomic force microscopy," *IEEE Trans. Ind. Electron.*, vol. 61, no. 7, pp. 3704–3712, Jul. 2014.

[2] H. C. Liaw and B. Shirinzadeh, "Robust adaptive constrained motion tracking control of piezo-actuated flexure-based mechanisms for micro/nano manipulation," *IEEE Trans. Ind. Electron.*, vol. 58, no. 4, pp. 1406–1415, Apr. 2011.

[3] M. Grossard, M. Boukallel, N. Chaillet, and C. Rotinat-Libersa, "Modeling and robust control strategy for a control-optimized piezoelectric microgripper," *IEEE/ASME Trans. Mechatronics*, vol. 16, no. 4, pp. 674–683, Aug. 2011.

[4] M. Karpelson, G.-Y. Wei, and R. J. Wood, "Driving high voltage piezoelectric actuators in microrobotic applications," *Sens. Actuators A, Phys.*, vol. 176, pp. 78–89, 2012.

[5] S. Li, J. Li, and Y. Mo, "Piezoelectric multimode vibration control for stiffened plate using ADRC-based acceleration compensation," *IEEE Trans. Ind. Electron.*, vol. 61, no. 12, pp. 6892–6902, Dec. 2014.

[6] Y. Li and Q. Xu, "Design and robust repetitive control of a new parallel-kinematic XY piezostage for micro/nanomanipulation," *IEEE/ASME Trans. Mechatronics*, vol. 17, no. 6, pp. 1120–1132, Dec. 2012.

[7] M. Al Janaideh, S. Rakheja, and C.-Y. Su, "An analytical generalized Prandtl–Ishlinskii model inversion for hysteresis compensation in micropositioning control," *IEEE/ASME Trans. Mechatronics*, vol. 16, no. 4, pp. 734–744, Aug. 2011.

[8] R. H. Comstock, "Charge control of piezoelectric actuators to reduce hysteresis effects," U.S. Patent 4 263 527, Apr. 21, 1981.

[9] C. Newcomb and I. Flinn, "Improving the linearity of piezoelectric ceramic actuators," *Electron. Lett.*, vol. 18, no. 11, pp. 442–444, 1982.

[10] J. Minase, T.-F. Lu, B. Cazzolato, and S. Grainger, "A review, supported by experimental results, of voltage, charge and capacitor insertion method for driving piezoelectric actuators," *Precis. Eng.*, vol. 34, no. 4, pp. 692–700, 2010.

[11] A. J. Fleming and S. R. Moheimani, "Precision current and charge amplifiers for driving highly capacitive piezoelectric loads," *Electron. Lett.*, vol. 39, no. 3, pp. 282–284, 2003.

[12] A. J. Fleming and S. R. Moheimani, "Improved current and charge amplifiers for driving piezoelectric loads, and issues in signal processing design for synthesis of shunt damping circuits," *J. Intell. Mater. Syst. Struct.*, vol. 15, no. 2, pp. 77–92, 2004.

[13] S. Devasia, E. Eleftheriou, and S. R. Moheimani, "A survey of control issues in nanopositioning," *IEEE Trans. Control Syst. Technol.*, vol. 15, no. 5, pp. 802–823, Sep. 2007.

[14] G. Song, J. Zhao, X. Zhou, and J. A. D. Abreu-García, "Tracking control of a piezoceramic actuator with hysteresis compensation using inverse Preisach model," *IEEE/ASME Trans. Mechatronics*, vol. 10, no. 2, pp. 198–209, Apr. 2005.

[15] L. Liu, K. K. Tan, S.-L. Chen, S. Huang, and T. H. Lee, "SVD-based Preisach hysteresis identification and composite control of piezo actuators," *ISA Trans.*, vol. 51, no. 3, pp. 430–438, 2012.

[16] H. Jiang, H. Ji, J. Qiu, and Y. Chen, "A modified Prandtl-Ishlinskii model for modeling asymmetric hysteresis of piezoelectric actuators," *IEEE Trans. Ultrason., Ferroelectr., Freq. Control*, vol. 57, no. 5, pp. 1200–1210, May 2010.

[17] G.-Y. Gu, L.-M. Zhu, and C.-Y. Su, "Modeling and compensation of asymmetric hysteresis nonlinearity for piezoceramic actuators with a modified Prandtl–Ishlinskii model," *IEEE Trans. Ind. Electron.*, vol. 61, no. 3, pp. 1583–1595, Mar. 2014.

[18] C.-Y. Su, Y. Feng, H. Hong, and X. Chen, "Adaptive control of system involving complex hysteretic nonlinearities: A generalised Prandtl–Ishlinskii modelling approach," *Int. J. Control*, vol. 82, no. 10, pp. 1786–1793, 2009.

[19] H. Sayyaadi and M. R. Zakerzadeh, "Position control of shape memory alloy actuator based on the generalized Prandtl–Ishlinskii inverse model," *Mechatronics*, vol. 22, no. 7, pp. 945–957, 2012.

[20] Q. Xu, "Identification and compensation of piezoelectric hysteresis without modeling hysteresis inverse," *IEEE Trans. Ind. Electron.*, vol. 60, no. 9, pp. 3927–3937, Sep. 2013.

[21] M. Rakotondrabe, "Bouc–Wen modeling and inverse multiplicative structure to compensate hysteresis nonlinearity in piezoelectric actuators," *IEEE Trans. Autom. Sci. Eng.*, vol. 8, no. 2, pp. 428–431, Apr. 2011.

[22] S. Bashash and N. Jalili, "A polynomial-based linear mapping strategy for feedforward compensation of hysteresis in piezoelectric actuators," *J. Dyn. Syst., Meas. Control*, vol. 130, no. 3, pp. 031008-1–031008-10, 2008.

[23] X. Tan and J. S. Baras, "Adaptive identification and control of hysteresis in smart materials," *IEEE Trans. Autom. Control*, vol. 50, no. 6, pp. 827–839, Jun. 2005.

[24] B. Ren, S. S. Ge, T. H. Lee, and C.-Y. Su, "Adaptive neural control for a class of nonlinear systems with uncertain hysteresis inputs and time-varying state delays," *IEEE Trans. Neural Netw.*, vol. 20, no. 7, pp. 1148–1164, Jul. 2009.
[25] B. Ren, S. S. Ge, C.-Y. Su, and T. H. Lee, "Adaptive neural control for a class of uncertain nonlinear systems in pure-feedback form with hysteresis input," *IEEE Trans. Syst., Man, Cybern. B, Cybern.*, vol. 39, no. 2, pp. 431–443, Apr. 2009.
[26] X. Chen and T. Hisayama, "Adaptive sliding-mode position control for piezo-actuated stage," *IEEE Trans. Ind. Electron.*, vol. 55, no. 11, pp. 3927–3934, Nov. 2008.
[27] Y. Wu and Q. Zou, "Robust inversion-based 2-DOF control design for output tracking: Piezoelectric-actuator example," *IEEE Trans. Control Syst. Technol.*, vol. 17, no. 5, pp. 1069–1082, Sep. 2009.
[28] C.-L. Hwang, "Microprocessor-based fuzzy decentralized control of 2-D piezo-driven systems," *IEEE Trans. Ind. Electron.*, vol. 55, no. 3, pp. 1411–1420, Mar. 2008.
[29] Q.-C. Zhong and D. Rees, "Control of uncertain LTI systems based on an uncertainty and disturbance estimator," *J. Dyn. Syst., Meas. Control*, vol. 126, no. 4, pp. 905–910, 2004.
[30] B. Ren, Q.-C. Zhong, and J. Chen, "Robust control for a class of non-affine nonlinear systems based on the uncertainty and disturbance estimator," *IEEE Trans. Ind. Electron.*, vol. 62, no. 9, pp. 5881–5888, Sep. 2015.
[31] W.-H. Chen, J. Yang, L. Guo, and S. Li, "Disturbance-observer-based control and related methods—An overview," *IEEE Trans. Ind. Electron.*, vol. 63, no. 2, pp. 1083–1095, Feb. 2016.
[32] S. Li, J. Yang, W.-H. Chen, and X. Chen, *Disturbance Observer-Based Control: Methods and Applications*. Boca Raton, FL, USA: CRC Press, 2014.
[33] J. Yi, S. Chang, and Y. Shen, "Disturbance-observer-based hysteresis compensation for piezoelectric actuators," *IEEE/ASME Trans. Mechatronics*, vol. 14, no. 4, pp. 456–464, Aug. 2009.
[34] S. Bashash and N. Jalili, "Robust multiple frequency trajectory tracking control of piezoelectrically driven micro/nanopositioning systems," *IEEE Trans. Control Syst. Technol.*, vol. 15, no. 5, pp. 867–878, Sep. 2007.
[35] M.-J. Yang, G.-Y. Gu, and L.-M. Zhu, "Parameter identification of the generalized Prandtl–Ishlinskii model for piezoelectric actuators using modified particle swarm optimization," *Sens. Actuators A, Phys.*, vol. 189, pp. 254–265, 2013.
[36] G.-Y. Gu, L.-M. Zhu, C.-Y. Su, and H. Ding, "Motion control of piezoelectric positioning stages: Modeling, controller design, and experimental evaluation," *IEEE/ASME Trans. Mechatronics*, vol. 18, no. 5, pp. 1459–1471, Oct. 2013.
[37] Q.-C. Zhong, A. Kuperman, and R. Stobart, "Design of UDE-based controllers from their two-degree-of-freedom nature," *Int. J. Robust Nonlinear Control*, vol. 21, no. 17, pp. 1994–2008, 2011.

Jinhao Chen (S'15) received the B.Eng. degree in information science and technology from Sun Yat-sen University (SYSU), Guangzhou, China, in 2012. He is currently working toward the Ph.D. degree in mechanical engineering at Texas Tech University, Lubbock, TX, USA.

His research interests include high-speed high-precision trajectory tracking control for piezoelectric systems, adaptive modeling-free control for actuators with hysteresis using uncertainty and disturbance estimation and compensation.

Beibei Ren (S'05–M'10) received the B.Eng. degree in mechanical and electronic engineering and the M.Eng. degree in automation from Xidian University, Xi'an, China, in 2001 and 2004, respectively, and the Ph.D. degree in electrical and computer engineering from the National University of Singapore, Singapore, in 2010.

From 2010 to 2013, she was a Post-Doctoral Scholar with the Department of Mechanical and Aerospace Engineering, University of California, San Diego, CA, USA. Since 2013, she has been an Assistant Professor with the Department of Mechanical Engineering, Texas Tech University, Lubbock, TX, USA. Her research interests include adaptive control, robust control, distributed parameter systems, extremum seeking, and their applications.

Qing-Chang Zhong (M'04–SM'04) received the Ph.D. degree in control and power engineering from Imperial College London, London, U.K., in 2004, and the Ph.D. degree in control theory and engineering from Shanghai Jiao Tong University, Shanghai, China, in 2000.

He is the Max McGraw Endowed Chair Professor of Energy and Power Engineering with the Department of Electrical and Computer Engineering, Illinois Institute of Technology, Chicago, IL, USA.

Prof. Zhong is a Distinguished Lecturer of both the IEEE Power Electronics Society and the IEEE Control Systems Society. He is a Fellow of the Institution of Engineering and Technology (IET), U.K., the Vice-Chair of the IFAC Technical Committee on Power and Energy Systems, and was a Senior Research Fellow of the Royal Academy of Engineering, U.K. (2009–2010), and the U.K. Representative to the European Control Association (2013–2015). He serves as an Associate Editor for the IEEE TRANSACTIONS ON AUTOMATIC CONTROL, IEEE TRANSACTIONS ON INDUSTRIAL ELECTRONICS, IEEE TRANSACTIONS ON POWER ELECTRONICS, IEEE TRANSACTIONS ON CONTROL SYSTEMS TECHNOLOGY, IEEE ACCESS, and IEEE JOURNAL OF EMERGING AND SELECTED TOPICS IN POWER ELECTRONICS. He was the recipient of the Best Doctoral Thesis Prize from Imperial College London in 2004.